

MCA-LLaVA: Manhattan Causal Attention for Reducing Hallucination in Large Vision-Language Models

Qiyao Zhao*
FKLPRIU, Xiamen University of
Technology, China
qiyanzhao618@gmail.com

Xiaofeng Zhang ‡*
Shanghai Jiao Tong University, China
SemiZxf@163.com

Yiheng Li
Nanyang Technological University,
Singapore
yiheng003@e.ntu.edu.sg

Yun Xing
Nanyang Technological University,
Singapore
xing0047@e.ntu.edu.sg

Xiaosong Yuan
Jilin University, China
yuanxs19@mails.jlu.edu.cn

Feilong Tang
Monash University, Australia
feilong.tang@monash.edu

Sinan Fan
Zhejiang University, China
222064@zju.edu.cn

Xuhang Chen
Huizhou University, China
xuhangc@hzu.edu.cn

Xu-Yao Zhang
Chinese Academy of Sciences, China
xyz@nlpr.ia.ac.cn

Da-Han Wang†
FKLPRIU, Xiamen University of
Technology, China
wangdh@xmut.edu.cn

Abstract

Hallucinations pose a significant challenge in Large Vision Language Models (LVLMs), with misalignment between multimodal features identified as a key contributing factor. This paper reveals the negative impact of the long-term decay in Rotary Position Encoding (RoPE), used for positional modeling in LVLMs, on multimodal alignment. Concretely, under long-term decay, instruction tokens exhibit uneven perception of image tokens located at different positions within the two-dimensional space: prioritizing image tokens from the bottom-right region since in the one-dimensional sequence, these tokens are positionally closer to the instruction tokens. This biased perception leads to insufficient image-instruction interaction and suboptimal multimodal alignment. We refer to this phenomenon as “image alignment bias.” To enhance instruction’s perception of image tokens at different spatial locations, we propose MCA-LLaVA, based on Manhattan distance, which extends the long-term decay to a two-dimensional, multi-directional spatial decay. MCA-LLaVA integrates the one-dimensional sequence order and two-dimensional spatial position of image tokens for positional modeling, mitigating hallucinations by alleviating image alignment bias. Experimental results of MCA-LLaVA across various hallucination and general benchmarks demonstrate its effectiveness and generality. The code can be accessed in <https://github.com/ErikZ719/MCA-LLaVA>.

*represents the co-first author. ‡represents project leader.

†represents the corresponding author. This work is supported by the Major Science and Technology Plan Project on the Future Industry Fields of Xiamen City (No. 3502Z20241027), the Unveiling and Leading Projects of Xiamen (No. 3502Z20241011), and the Open Project of the State Key Laboratory of Multimodal Artificial Intelligence Systems (MAIS2024101).

Conference’17, Washington, DC, USA
2025. ACM ISBN 978-x-xxxx-xxxx-x/YYYY/MM
<https://doi.org/10.1145/nnnnnnn.nnnnnnn>

CCS Concepts

• **Computing methodologies** → **Computer vision tasks**.

Keywords

Large Vision Language Models, Hallucination, Rotary Position Encoding, Long-term Decay, Multimodal Alignment

ACM Reference Format:

Qiyao Zhao, Xiaofeng Zhang ‡, Yiheng Li, Yun Xing, Xiaosong Yuan, Feilong Tang, Sinan Fan, Xuhang Chen, Xu-Yao Zhang, and Da-Han Wang. 2025. MCA-LLaVA: Manhattan Causal Attention for Reducing Hallucination in Large Vision-Language Models. In . ACM, New York, NY, USA, 10 pages. <https://doi.org/10.1145/nnnnnnn.nnnnnnn>

1 Introduction

Large Vision-Language Models (LVLMs) [1, 3, 9, 38, 39, 61, 69, 79] have demonstrated impressive multimodal understanding across various domains, such as document comprehension [24, 43] and complex visual reasoning [71]. However, the reliability of LVLMs is compromised by hallucinations [34, 46], a phenomenon in which models generate counterfactual responses that do not align with the information from the question image.

Recent studies [4, 40, 41] have identified the misalignment between visual and textual inputs as a key contributor to hallucinations. In particular, widely used Large Vision-Language Models (LVLMs) typically project encoded visual features into the textual embedding space of Large Language Models (LLMs) [55]. However, the inherent distribution gap between visual and textual tokens poses significant challenges for cross-modal interaction and feature alignment. To address this issue and reduce hallucinations, several approaches have focused on enhancing modality alignment through improved alignment training, such as augmenting fine-grained data for instruction fine-tuning [37], or applying reinforcement learning

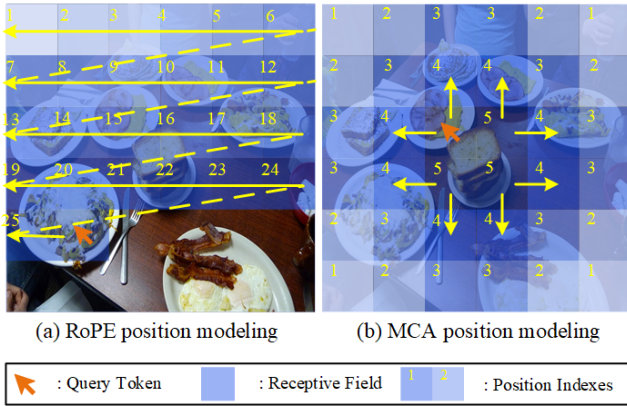


Figure 1: Schematic of long-term decay in different positional encoding mechanisms. Yellow arrows indicate the direction of decay. In the causal attention mechanism, the direction of decay always goes from tokens with larger position indices to tokens with smaller position indices. (a) denotes RoPE one-dimensional unidirectional long-term decay. (b) denotes MCA spatial multi-directional long-term decay. Darker colors represent smaller decay, while lighter colors represent larger decay. The number of encoded image tokens is set to 36 for the demonstration.

guided by human feedback [51]. More recently, a series of contrastive decoding strategies [30, 62, 87] has been introduced to mitigate hallucinations during inference without additional training. Although these methods offer partial relief, the internal mechanisms within the models that lead to modality misalignment and hallucinations remain insufficiently understood.

Recent research focusing on information flow has provided insight into relationship between hallucinations and LVLMs internal mechanisms. Label Words [60] first combines the attention value and gradient to identify attention sink observing that the information flow always converges to the prompt token eventually. OPERA[22] attributed object hallucination to some prompt tokens that receive consistently high attention at the decoding stage. EAH[80] found that input image tokens with high-density information flow in some attention heads can help mitigate hallucination. Leveraging information flow, these studies clarify the relationship between prompt tokens, image tokens, and hallucinations. However, the information flow between tokens of different modalities remains to be explored. A deeper exploration of multimodal information flow may help to reflect the multimodal alignment process in LVLMs.

Unlike previous work, this paper delves into RoPE [50], a key component for position modeling in LVLMs, examining its negative impact on multimodal alignment and its relationship with hallucinations.

Q1: Is long-term decay of RoPE suitable for multimodal alignment?

Under RoPE long-term decay, varying levels of attention are assigned to image tokens based on their relative distances from instruction tokens, with those farther away receiving less attention. To investigate information interaction under long-term decay, we

visualize the image-to-instruction information flow, as shown in Figure 2.a. We found that only the tokens in the lower-right region of the image exhibited dense information flow due to their proximity to the instruction tokens in the one-dimensional sequence, while a large number of image tokens, distant from the instruction tokens, showed very sparse information flow. This imbalanced distribution of information flow further reveals the model’s uneven perception: only image tokens in a limited region interact sufficiently with the instruction tokens, which hinders multimodal alignment and leads to hallucinations. We refer to this phenomenon as “image alignment bias” and provide a detailed explanation in Section 3.

Q2: What limits the long-term decay of RoPE in multimodal alignment?

CCA-LLaVA [66] is the first to find that LVLMs may be more prone to hallucinations because of long-term decay. To this end, it heuristically redirects instruction tokens to focus more on the image center region by reassigning the image tokens’ position indices in the form of concentric squares. Distinct from CCA, we observe that long-term decay disregards the two-dimensional position of the image, considering only the image tokens’ position in the one-dimensional sequence when calculating relative distances. As shown in Figure 1.a, this distance-dependent decay aligns with the order distribution of information in a 1D text sequence but overlooks the spatial distribution of information in a 2D image. Therefore, our goal is to extend the long-term decay to the two-dimensional spatial domain, calculating the relative positional distances of image tokens based on spatial locality. This enhances the model’s perception of image tokens at different spatial locations.

To this end, we propose Manhattan Causal Attention (MCA) to mitigate hallucination in LVLMs caused by RoPE long-term decay. MCA consists of three key designs: 1. The RoPE one-dimensional long-term decay is evolved into the two-dimensional, multi-directional spatial decay by calculating the Manhattan distance between tokens; 2. We reassign the two-dimensional position coordinates of image tokens to align with the Manhattan distance computation. After that we replace the RoPE raster-scan position indices with new position indices, which are computed based on position coordinates; 3. Modeling image position dependency by Manhattan causal mask module, which preserves 2D spatial localization properties.

We evaluated the MCA extensively: compared to the baseline, MCA improves F1 scores by +6.7% and Accuracy by +6.7% on POPE, and reduces sentence-level hallucination by 9% and instance-level hallucination by 2.9% on CHAIR. Additionally, our approach enhances overall image perception and information interaction, showing promising performance on several general tasks such as MME and SQA. Experimental results across multiple hallucination benchmarks and a range of LVLMs show the consistent improvements brought by MCA. Our contribution consists of three parts:

- This paper delves into the relationship between RoPE and hallucinations. We reveal the image alignment bias, arising from RoPE long-term decay, leads to inferior multimodal alignment and hallucinations.
- We propose Manhattan Causal Attention, which models image position dependency by Manhattan relative position

distance. MCA extends the long-term decay to the 2-D multi-directional spatial decay, which mitigates hallucinations caused by image alignment bias.

- Experiments on both hallucination and general benchmarks demonstrate the promising performance of our design.

2 Related Work

2.1 Hallucination in LVLMS

Hallucination in Large Vision-Language Models (LVLMS) refers to the phenomenon in which the model’s textual output contradicts the visual input, such as generating descriptions that include objects or attributes not present from the image [29, 34, 46, 74]. Most existing LVLMS project encoded visual features into the input space of the language model; however, a significant modality gap between textual and visual tokens often results in cross-modal misalignment, leading to hallucinations during generation [4, 19, 35, 40, 84]. Several studies have sought to improve cross-modal alignment interfaces to reduce hallucination risks [9, 21, 38, 48], while others have employed contrastive learning strategies to enhance alignment between visual and textual representations [26, 36, 47]. Additional approaches have leveraged diverse, fine-grained fine-tuning datasets [6, 29, 37, 59, 72, 78] or human feedback alignment [51, 73], though these typically incur high annotation costs. Recently, a range of decoding strategies has been proposed to mitigate hallucinations by intervening in the model’s reasoning process without requiring further training [5, 17, 27, 28, 30, 58, 62, 87]; however, these methods do not improve intrinsic modal alignment and often reduce inference efficiency. Preference optimization techniques, which train models based on comparisons between positive and negative samples, have also been explored [13, 16, 44, 57, 63, 65, 67, 85], though these are often prone to overfitting on specific datasets. Recent research has further revealed that LVLMS exhibit attention bias between image and text modalities [41, 66, 70, 88], where insufficient visual perception contributes to hallucination. Some methods address this issue by correcting attention distribution bias in a training-free manner [2, 52, 54, 68, 70, 80], while others adopt fine-tuning strategies to enhance multimodal alignment [66, 89]. These approaches have demonstrated improved attention to visual input. In contrast to the above methods, this paper investigates the impact of RoPE’s long-term decay on cross-modal alignment, from the perspective of positional modeling mechanisms in LVLMS.

2.2 Information Flow in LVLMS

With the rapid development of LVLMS[1, 3, 32, 45, 61, 77], more and more works try to find inspiration for model optimization by analyzing the internal mechanisms of the models. Among these, information flow [8, 60, 82, 83] provides an intuitive method to understand the internal mechanisms of LVLMS black-box models. Label Words [60], and ACT [75] are early works that explore the mechanism of LLMs[14, 55, 86] through observing information flow patterns. By calculating saliency scores, it is possible to visualize the information flow.

Building on this, OPERA [22] and DOPRA [64] introduced information flow to reveal the relationship between token attention value and hallucinations. They found that during the decoding of LVLMS, some special tokens (e.g., “-”, “?”) receive consistently high

attentional values, which leads to hallucinations. To this end, they propose different penalty constraints to alleviate the over-reliance on these tokens. LLaVA-CAM [81] combines Grad-CAM and attention map to propose a dynamic analysis of information flow, which reveals the fine-grained effect of token in the LVLMS prediction. EAH [80] analyzed the information flow of image tokens across each layer and head of the LVLMS. It proposes a train-free method to enhance the information flow distribution of image tokens in specific layers to improve the image perception of the model.

2.3 Position Encoding in LVLMS

Position encoding was first proposed for Transformer[56] sequence tokens position dependency modeling. To enable LVLMS to understand the order information of tokens, different methods have been proposed to encode position information into representations. Commonly used position encoding includes absolute position encoding[56], learnable position encoding[15], and relative position encoding[23]. QwenVL2[61] proposes Multimodal Rotary Position Embedding to incorporate temporal information into the position representation. Among them, RoPE[50] encodes positional representation for linear attention using rotation matrices and is widely used in LVLMS. This paper provides an in-depth analysis of the relationship between RoPE and hallucination phenomenon and reveals the limitations of the relative position calculation.

2.4 Image Alignment Bias

In this section, we first analyze the phenomenon of image alignment bias triggered by the RoPE long-term decay. By further analyzing the image-to-instruction information flow, we reveal the negative effects of image alignment bias on multimodal alignment and hallucination. Finally, we clarify the causes and limitations of the image alignment bias from the perspective of the RoPE positional encoding mechanism.

Long-term decay causes image alignment bias: Under the long-term decay induced by RoPE, target tokens positioned farther from an instruction token experience greater decay in their attention scores [50]. This decay aligns with the typical distribution of information in language modeling, wherein text is represented as a one-dimensional sequence and tokens closer in relative position to the query token generally carry more consistent and semantically relevant information.

In LVLMS, image tokens are flattened into a 1-D sequence using a raster-scan order (top-to-bottom, left-to-right) and concatenated with instruction tokens to form the input sequence. Due to RoPE’s decay effect, attention toward image tokens positioned farther from the instruction tokens decays progressively. This results in a fixed multimodal alignment pattern in which instruction tokens predominantly attend to image tokens located later in the raster-scan order, while tokens earlier in the sequence receive limited attention, as illustrated in Figure 1.a. We term this phenomenon as image alignment bias, which is a systemic bias introduced into the visual feature attention by the internal mechanisms of LVLMS, rather than an attention pattern learned based on training.

Information flow for image alignment bias: We visualize the image-to-instruction information flow to examine the impact of

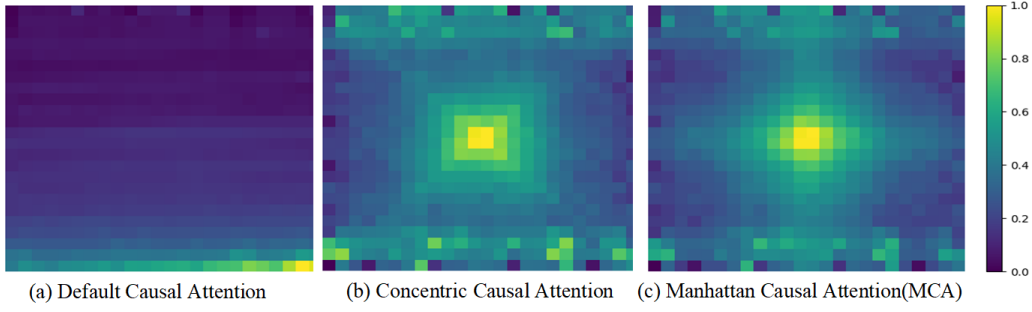


Figure 2: (a), (b), and (c) show the information flow of image-to-instruction in LLaVA1.5[38], CCA[66], and MCA, respectively. We aggregate the information flow of each image token in the input tokens to the instruction tokens, and the aggregation results are arranged according to the corresponding positions of the image tokens in the 2-D space. The reported statistics are averaged over the 3K adversarial subset used for evaluation in the POPE [34].

image alignment bias on multimodal alignment. As shown in Figure 2.a, we find that image tokens in the lower-right region, which are closer to the instruction token, exhibit dense information flow, while the majority of image tokens in other regions exhibit sparse information flow. This suggests that many image tokens fail to interact sufficiently with instruction token, which leads to multimodal misalignment and hallucinations.

This extreme information flow distribution hinders the model’s perception of overall image information. CCA was the first to identify a similar phenomenon, confirming that LVLs are more likely to generate hallucinations when relevant visual cues are positioned far from instruction tokens within the multimodal input sequence. To mitigate this issue, a heuristic reallocation of visual attention was proposed. However, this approach lacks interpretability with respect to the internal mechanisms of LVLs. In this work, the underlying causes of unbalanced information flow and image alignment bias are analyzed through the lens of RoPE long-term decay. **Ignoring the spatial properties of the image in relative position calculations during long-term decay:** Given a multimodal input sequence of LVLs, Q_i is the instruction query token at position i and K_j is the image key token at position j . To model the relative position dependency among them, RoPE multiplies the Q_i and K_j with the rotation matrix via $R_{\theta,i}^d \cdot Q_i$ and $R_{\theta,j}^d \cdot K_j$. The rotation matrix $R_{\theta,m}^d$ is shown in Eq. 1, where

$$R_{\theta,m}^d = \begin{pmatrix} \cos(m\theta_1) & -\sin(m\theta_1) & 0 & 0 & \dots & 0 & 0 \\ \sin(m\theta_1) & \cos(m\theta_1) & 0 & 0 & \dots & 0 & 0 \\ 0 & 0 & \cos(m\theta_2) & -\sin(m\theta_2) & \dots & 0 & 0 \\ 0 & 0 & \sin(m\theta_2) & \cos(m\theta_2) & \dots & 0 & 0 \\ \vdots & \vdots & \vdots & \vdots & \ddots & \vdots & \vdots \\ 0 & 0 & 0 & 0 & \dots & \cos(m\theta_{d/2}) & -\sin(m\theta_{d/2}) \\ 0 & 0 & 0 & 0 & \dots & \sin(m\theta_{d/2}) & \cos(m\theta_{d/2}) \end{pmatrix} \quad (1)$$

$\{\theta_i = 10000^{-2(i-1)/d}\}$, $i \in (1, 2, \dots, d/2)$ denotes the predefined sinusoidal function values, d denotes the embedding dimension, and m denotes the position index. The attention value $Attn$ between Q_i and K_j is calculated as follows:

$$Attn_{i,j} = \text{softmax} \left(\frac{Q_i^T \cdot (R_{\theta,i}^d)^T \cdot R_{\theta,j}^d \cdot K_j}{\sqrt{d}} \right) = \text{softmax} \left(\frac{Q_i^T \cdot R_{\theta,(j-i)}^d \cdot K_j}{\sqrt{d}} \right) \quad (2)$$

The $Attn$ reflects the degree of long-term decay: As the relative distance $j - i$ between image and instruction tokens increases, the attention $Attn$ gradually decreases. In calculating relative distances, image tokens are assigned position indices based on their order in a 1-D sequence after flattening, ignoring their 2-D spatial positions. As a result, the long-term decay induces image alignment bias.

3 Manhattan Causal Attention

To mitigate the object hallucination caused by the RoPE image alignment bias, we propose the Manhattan Causal Attention (MCA). MCA consists of three parts: 1. Relative position distance computation evolves from one-dimensional to two-dimensional Manhattan distances, preserving the spatial nature of the image; 2. Assigning position coordinates to each image token and merging the position coordinates as new position indexes; and 3. Modify the default causal attention masking to Manhattan causal masking.

3.1 Manhattan Relative Position Distance

As shown in Eq. 3, RoPE models the relative

$$D_{RoPE}\{Q_i, K_j\} = \gamma(j) - \gamma(i) \quad (3)$$

distance between Q_i and K_j as $\gamma(j) - \gamma(i)$. γ denotes the position index under raster scanning. This approach limits the relative positional distances of image tokens to the one-dimensional level and loses the spatial locality of the two-dimensional image.

To address this limitation, we extend the computation of the relative positional distance of image tokens to two-dimensional levels. Naturally, the image tokens at position m can correspond to a coordinate in two-dimensional space (x_m, y_m) . Therefore we expand the one-dimensional relative positional distance (Eq. 3) to the two-dimensional Manhattan relative positional distance (Eq. 4) between the image tokens coordinates.

$$D_{Manhattan}\{Q_i, K_j\} = (x_j - x_i) + (y_j - y_i) \quad (4)$$

From Position indexes to Position Coordinates: Under raster scan, image tokens are scanned row by row starting from the top

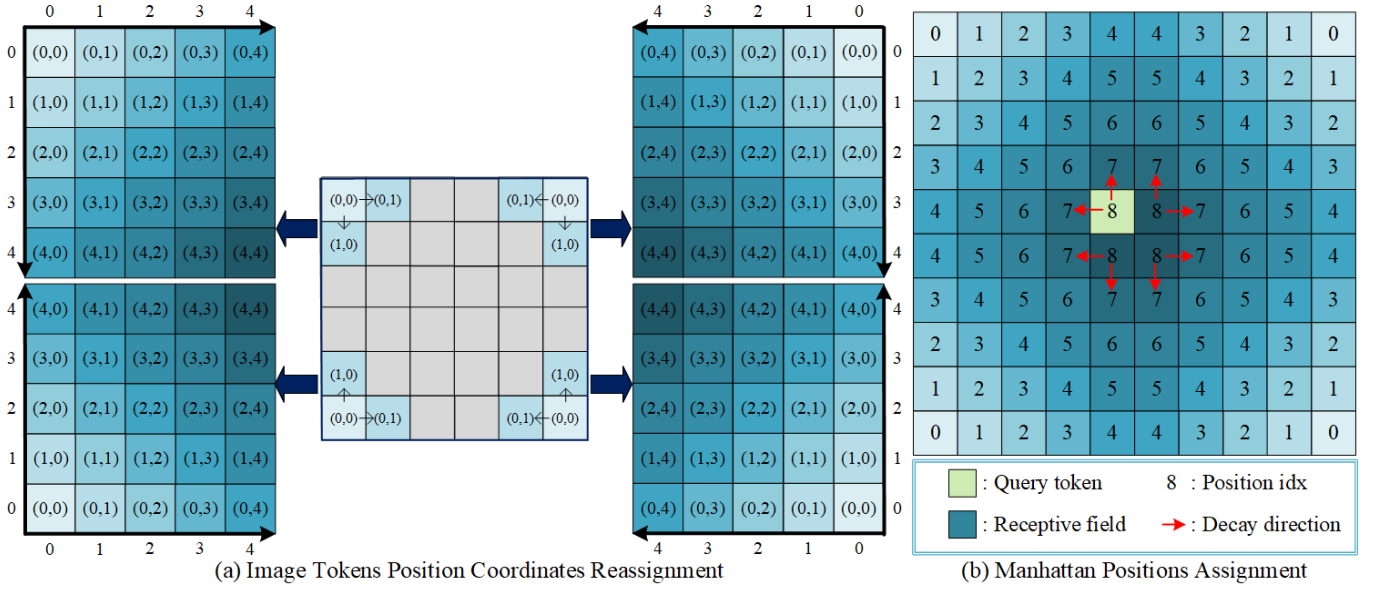


Figure 3: Illustration of image token position coordinate reassignment. The total number of image tokens is denoted as V ; for demonstration purposes, $V = 100$, while the default setting in LLaVA-1.5 uses $V = 576$. The image tokens are mirrored into four partitions, with the four vertex positions designated as origins. Subsequently, two-dimensional positional coordinates are assigned sequentially to the remaining visual tokens based on the direction of the coordinate axes shown in (a). (b) shows the new position index computed from the coordinates.

left and assigned position indexes with increments of 1 as follows:

$$\begin{bmatrix}
 0 & 1 & \dots & \sqrt{v}-2 & \sqrt{v}-1 \\
 \sqrt{v} & \sqrt{v}+1 & \dots & 2\sqrt{v}-2 & 2\sqrt{v}-1 \\
 & & \ddots & & \\
 \vdots & \vdots & \frac{v}{2}-\frac{\sqrt{v}}{2}-1 & \frac{v}{2}-\frac{\sqrt{v}}{2} & \vdots \\
 \vdots & \vdots & \frac{v}{2}+\frac{\sqrt{v}}{2}-1 & \frac{v}{2}+\frac{\sqrt{v}}{2} & \vdots \\
 & & & & \ddots \\
 v-2\sqrt{v} & v-2\sqrt{v}+1 & \dots & v-\sqrt{v}-2 & v-\sqrt{v}-1 \\
 v-\sqrt{v} & v-\sqrt{v}+1 & \dots & v-2 & v-1
 \end{bmatrix} \quad (5)$$

where v denotes the number of image tokens. Since adding column coordinates directly to the position index cannot compute $D_{Manhattan}$ correctly, we reassign coordinates to the image tokens.

Specifically, the tokens at the four vertices of the image are set as the origin points with coordinate $(0, 0)$. As shown in Figure 3.a, tokens adjacent to the origin points are treated as next tokens with an increment of 1. The positive direction of the horizontal and vertical coordinate axes is defined according to the incremental direction. The final image tokens' position coordinates are as follows:

$$\begin{bmatrix}
 (0,0) & (0,1) & \dots & (0,\frac{\sqrt{v}}{2}-1) & (0,\frac{\sqrt{v}}{2}-1) & \dots & (0,1) & (0,0) \\
 (1,0) & (1,1) & \dots & (1,\frac{\sqrt{v}}{2}-1) & (1,\frac{\sqrt{v}}{2}-1) & \dots & (1,1) & (1,0) \\
 \vdots & \vdots & \ddots & \vdots & \vdots & \ddots & \vdots & \vdots \\
 (\frac{\sqrt{v}}{2}-1,0) & (\frac{\sqrt{v}}{2}-1,1) & \dots & (\frac{\sqrt{v}}{2}-1,\frac{\sqrt{v}}{2}-1) & (\frac{\sqrt{v}}{2}-1,\frac{\sqrt{v}}{2}-1) & \dots & (\frac{\sqrt{v}}{2}-1,1) & (\frac{\sqrt{v}}{2}-1,0) \\
 (\frac{\sqrt{v}}{2}-1,0) & (\frac{\sqrt{v}}{2}-1,1) & \dots & (\frac{\sqrt{v}}{2}-1,\frac{\sqrt{v}}{2}-1) & (\frac{\sqrt{v}}{2}-1,\frac{\sqrt{v}}{2}-1) & \dots & (\frac{\sqrt{v}}{2}-1,1) & (\frac{\sqrt{v}}{2}-1,0) \\
 \vdots & \vdots & \ddots & \vdots & \vdots & \ddots & \vdots & \vdots \\
 (1,0) & (1,1) & \dots & (1,\frac{\sqrt{v}}{2}-1) & (1,\frac{\sqrt{v}}{2}-1) & \dots & (1,1) & (1,0) \\
 (0,0) & (0,1) & \dots & (0,\frac{\sqrt{v}}{2}-1) & (0,\frac{\sqrt{v}}{2}-1) & \dots & (0,1) & (0,0)
 \end{bmatrix} \quad (6)$$

The $V \times V$ image tokens are divided into four parts of the mirror image according to the four origin points, and each part consists

of $\frac{\sqrt{v}}{2} \times \frac{\sqrt{v}}{2}$ tokens. In each part, the token's position coordinates are linearly incremented in the positive direction along the two-dimensional coordinate axis of the origin point, which preserves the two-dimensional localized spatial characteristics of images.

3.2 Manhattan Positions Assignment

We note that by replacing the positional index of the raster-scan with the sum of the coordinate values of the tokens, the Manhattan relative positional distance can be formally aligned with Eq. 3.

$$\begin{cases} \mu(m) = x_m + y_m \\ D_{Manhattan}\{Q_i, K_j\} = \mu(j) - \mu(i) \end{cases} \quad (7)$$

Therefore, we use the sum of token coordinates as new position indexes, termed Manhattan positions assignment μ , to adapt the calculation of the relative positional distance of Manhattan. As shown in Figure 3.b, Manhattan position assignment preserves the local spatial properties of the image: causal attention of image tokens extends from unidirectional ROPE decay to multidirectional decay. Additionally, compared to raster scanning, the number of Manhattan Position indexes decreases from V to $\sqrt{v}-1$, which reduces the overall distance between image and instruction tokens. This is more favorable for information interaction[66].

3.3 Manhattan Causal Masking

The default causal attention scores $Attn$ between Q_i and K_j are calculated by Eq.2. We propose MCA to model the relative positions

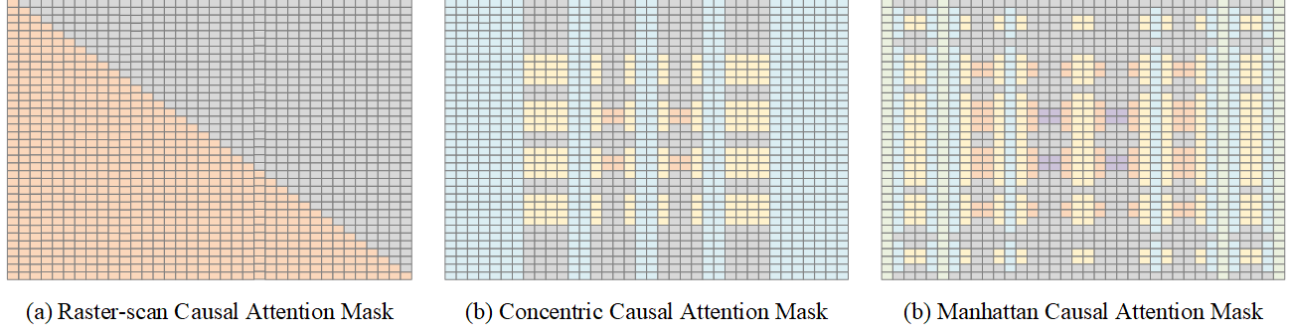


Figure 4: The default causal masks are $V \times V$. We show the causal masks when the number of image tokens V is 36. By default causal modeling in (a), image tokens focus on all visual tokens in between; by CCA in (b), the central image tokens focus on peripheral tokens; and by MCA in (c), image tokens focus on neighboring image tokens in four directions.

of tokens by 2D Manhattan distance, updating $Attn$ to $Attn'$:

$$Attn'_{i,j} = \text{softmax} \left(\frac{Q_i^T \cdot \left(R_{\theta, (x_i, y_i)}^d \right)^T \cdot R_{\theta, (x_j, y_j)}^d \cdot K_j}{\sqrt{d}} \right) = \text{softmax} \left(\frac{Q_i^T \cdot R_{\theta, (x_j - x_i) + (y_j - y_i)}^d \cdot K_j}{\sqrt{d}} \right) \quad (8)$$

By Manhattan position assignment and constant transformation (Eq. 7), $Attn'$ is formally unified with $Attn$. We follow the principle of default causal attention, where the query token Q_i can only attend to the previous key tokens $\{K_j, j \leq i\}$ in the sequence during causal attention masking, shown in Figure 4.a. Our Manhattan causal masking is presented in Figure 4.c. For the two-dimensional continuity information contained in images, we preserve spatial localization properties when modeling causal attributes, mitigating object hallucination triggered by image observation bias.

4 Experiment

MCA was evaluated on popular hallucination benchmarks, including POPE and CHAIR, as well as general-purpose benchmarks, such as GQA, VQA, MME, SQA, etc. Results show that MCA improves overall visual information perception in LVLs, rather than overfitting to hallucination-specific datasets. LLaVA-1.5-7B was used as the baseline LVL, and MCA was further extended to different model architectures (e.g., InternVL-7B) and larger model sizes (e.g., LLaVA-1.5-13B) to verify the robustness. Ablation studies on different positional encoding methods and MCA variants further confirm the effectiveness of the proposed approach.

4.1 Experimental Setup and Dataset

Training Details. All experiments are performed on an 8xA800. The visual encoder uses the pre-trained CLIP[45] ViT-L/14 and the LLM uses Vicuna-7B[11]. We adopt two-stage training: pre-training stage on CC-558K dataset[39] with 1 epoch and 256 batch size; instruction tuning stage on 665k multi-turn conversation dataset[38] with 1 epoch and 128 batch size.

4.2 Evaluation Results of MCA-LLaVA on Hallucination Benchmark

Evaluation Benchmarks. POPE[34] evaluates LVLs hallucination through object-level question-answering tasks. Check whether the model correctly identifies the presence of a specific object in

Methods	POPE		CHAIR			
	<i>F1-score</i> ↑	<i>acc</i> ↑	C_S ↓	C_I ↓	<i>Recall</i> ↑	<i>Avg. Len</i>
Greedy Search	79.3	79.8	47.0	13.8	76.6	94.2
Beam Search	84.9	86.0	51.0	15.2	75.2	102.2
DoLa [12]	80.2	83.1	57.0	15.2	78.2	97.5
ITI [33]	83.7	84.9	48.2	13.9	78.3	98.6
VCD [30]	83.2	82.0	51.0	14.9	77.2	101.9
OPERA [22]	85.2	84.2	47.0	14.6	78.5	95.3
DOPRA [64]	85.6	84.3	46.3	13.8	78.2	96.1
HALC [10]	83.9	84.0	50.2	12.4	78.4	97.2
Less is more [76]	86.0	86.8	40.2	12.3	75.7	79.7
CCA-LLaVA [66]	85.9	86.5	43.0	11.5	80.4	96.6
TAME [53]	85.5	85.9	45.2	14.0	74.4	98.8
SID [25]	85.6	85.8	44.2	12.2	73.0	99.4
MCA-LLaVA	86.0	86.5	38.0	10.9	76.6	92.5

Table 1: Compare results of MCA with other SOTA methods on POPE and CHAIR datasets. We report the average $F1$ – score computed on random, popular, and adversarial splits of POPE (baseline: LLaVA-1.5-7B), max-tokens=512. The best performances within each setting are bolded.

the image by querying prompts like "Is there a <object> in the image?". CHAIR [46] evaluates LVLs hallucination through object-level image captioning tasks. It includes two evaluation aspects: instance-level hallucinations $CHAIR_I$ (C_I) and sentence-level hallucinations $CHAIR_S$ (C_S), calculated as follows:

$$C_S = \frac{|\{\text{hallucinated objects}\}|}{|\{\text{all mentioned objects}\}|} \quad (9)$$

$$C_I = \frac{|\{\text{captions w/ hallucinated objects}\}|}{|\{\text{all captions}\}|} \quad (10)$$

Effectiveness of MCA-LLaVA. In this paper, the POPE and CHAIR scores of LLaVA1.5-7b under greedy search are used as the baseline results. According to Section 4.2, we replaced the image position index determined by the RoPE raster-scan with the Manhattan positions assignment. This approach introduces spatial priors to RoPE long-term decay, and achieves a 6.7% improvement in $F1$ score and a 6.7% improvement in accuracy on POPE, as shown in Table 1. We hypothesize that MCA-LLaVA alleviates image observation bias, allowing the instruction tokens to focus more effectively on the image information. Compared with other state-of-the-art hallucination mitigation methods, the MCA-LLaVA obtained the highest $F1$ score of 86.0% and the second highest accuracy of 86.5% on POPE.

Model	GQA	VizWiz	SQA [†]	MMB	MMStar	VQA ^{v2}	SEED ^A	SEED ^I	SEED ^V
LLaVA1.5-7B	62.0	50.0	66.8	64.3	30.0	78.5	58.6	66.1	37.3
VCD	61.9	50.5	68.5	-	34.6	58.3	63.7	37.6	
CCA-LLaVA	63.5	53.7	67.3	64.0	33.2	-	61.7	67.1	41.0
MCA-LLaVA	63.0(+1.0)	53.6(+3.6)	68.7(+3.5)	65.8(+1.5)	36.5(+6.5)	78.9(+0.1)	62.1(+3.5)	67.9(+1.8)	41.3(+4.0)

Table 2: Performance comparison on six general vision-language tasks. These benchmarks include multiple-choice questions from different domains. The experiments were conducted using lmms-eval on A800.

Methods	Object-level		Attribute-level		Total Score [↑]
	Existence [↑]	Count [↑]	Position [↑]	Color [↑]	
Beam	175.67	124.67	114.00	151.00	565.34
Greedy	185.00	93.33	110.00	156.67	545.00
DOLA [12]	175.00	108.33	90.00	138.33	511.66
VCD [30]	184.66	138.33	128.67	153.00	604.66
OPERA [22]	180.67	133.33	123.33	155.00	592.33
CCA-LLaVA[66]	190.00	148.33	128.33	175.00	641.66
SID [25]	182.00	127.00	116.00	139.00	564.00
TAME+OPERA [53]	176.00	118.33	113.00	143.00	550.33
MCA-LLaVA (Our)	190.00	163.33	126.67	170.00	650.00

Table 3: Evaluation results on the hallucination subset of MME [71]. The best performances within each setting are bolded, baseline: LLaVA1.5-7B.

For CHAIR, we set the maximum number of generated response tokens to 512 to evaluate the generated long captions hallucinations. It is important to note that longer responses better reflect the model’s perception of the image information. As shown in Table 1, MCA-LLaVA achieves the best C_I and C_S among all SOTA methods. Under greedy search, our model improves 9% at the sentence level and 2.9% at the instance level compared to the baseline. These results demonstrate the importance of optimizing RoPE image tokens position modeling for mitigating hallucinations.

4.3 Evaluation Results of MCA-LLaVA on General Vision-language Benchmarks

Evaluation Benchmarks. We also evaluate MCA-LLaVA on more visual-language benchmarks, including general visual-linguistic tasks and vision-centered tasks such as MME-Bench [71], VizWiz [20], MMSTAR [7], GQA [24], SEED[31], TextVQA[49], VQAv2[18], and ScienceQA [42].

Effectiveness of MCA-LLaVA. MME evaluates the overall image perception ability of the model, revealing hallucinations from a broader perspective, not just object hallucinations. We analyze the object-level and attribute-level hallucinations of LVLMS from four types of metrics: object existence, count, position, and color. We report the results of MCA-LLaVA on MME in Table 3. MCA-LLaVA outperforms the baseline model in all four evaluation metrics, with a total score improvement of 105 compared to the baseline. Additionally, MCA-LLaVA showed better image perception and total score compared to other SOTA. Notably, our method outperforms CCA-LLaVA by 15 on the Count metric, indicating that our approach can perceive the overall image information at a finer granularity. The qualitative examples in Figure 5 reveal the hallucinations generated by CCA-LLaVA in analyzing object counts in graphical scenes.

To evaluate the model’s general perception ability beyond hallucinations, we tested the performance of MCA-LLaVA on eight general vision-language tasks using lmms-eval. These benchmarks

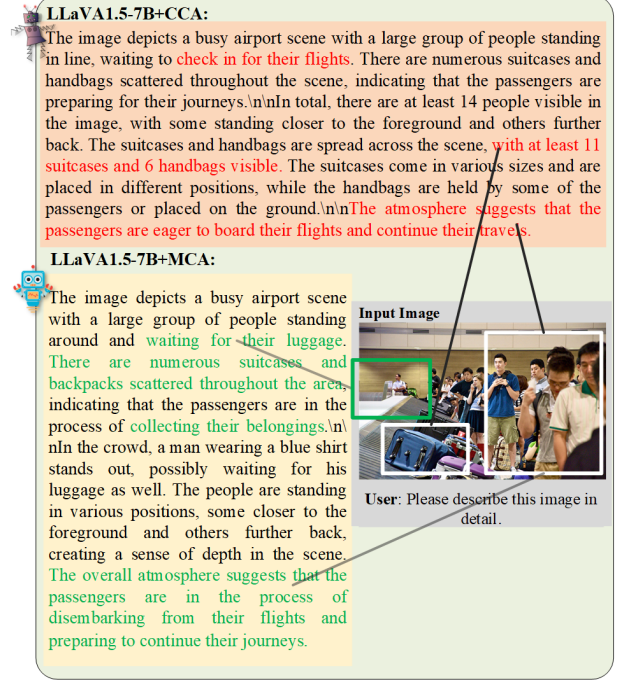


Figure 5: Qualitative results of CCA-LLaVA with MCA-LLaVA. Our method generate less hallucinations.

evaluate the model through multiple-choice questions, covering topics such as scientific knowledge, complex reasoning, and more. As shown in table 2, MCA-LLaVA demonstrates consistent performance improvements across all benchmarks, such as a 1.5% and 6.5% increase over the baseline on MMB and MMStar, respectively. The experimental results demonstrate that MCA-LLaVA enhances the model’s image perception ability comprehensively by mitigating image bias, rather than overfitting to hallucination benchmarks.

4.4 Results of MCA-LLaVA with CCA-LLaVA

As shown in Figure 5, the description generated by CCA-LLaVA contains hallucinated elements. It focuses on the people queuing at airports but incorrectly describes the process of preparing passengers to board a plane. Additionally, the generated response contains two incorrect descriptions of item quantities: 11 suitcases and 6 handbags. This reveals the model’s insufficient understanding of the global image information.

On the other hand, MCA-LLaVA’s description correctly states the fact that people are waiting to collect their luggage. This suggests that MCA-LLaVA better integrates the overall image information

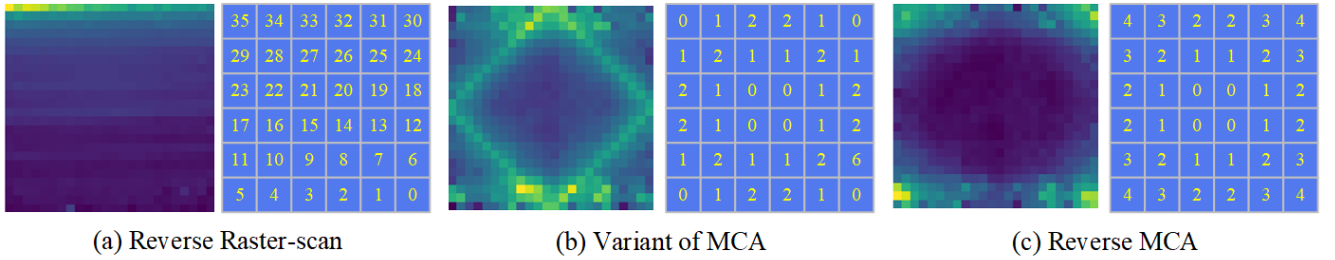


Figure 6: Different positional indices and corresponding information flow patterns.

Method	POPE		CHAIR		
	F1 score \uparrow	acc \uparrow	$C_S \downarrow$	$C_I \downarrow$	Recall \uparrow
LLaVA-1.5-7B	79.3	79.8	47.0	13.8	76.6
MCA	86.0 (+6.7)	86.5 (+6.7)	38.0 (+9.0)	10.9 (+2.9)	76.6
LLaVA-1.5-13B	82.4	82.7	44.0	12.7	77.3
MCA	85.9 (+3.5)	86.1 (+3.4)	37.2 (+6.8)	10.3 (+2.4)	78.0
InternVL-7B	81.6	82.2	45.8	12.9	79.1
MCA	83.1 (+1.5)	83.6 (+1.4)	44.9 (+0.9)	12.3 (+0.6)	80.3

Table 4: Generalization study of MCA on other LVLMS.

and understands the context of disembarking from the plane. Additionally, MCA-LLaVA’s description mentions objects that CCA-LLaVA does not, such as a man in a blue shirt and backpack. This indicates that MCA-LLaVA is capable of observing richer and more fine-grained image information.

4.5 Ablation Study

Generalization Study of MCA To further validate the robustness of the proposed method, MCA was applied to additional LVLMS. Similar to the baseline model LLaVA-1.5-7B, InternVL-7B also adopts a RoPE-based positional modeling mechanism. InternVL leverages LLaMA2 to construct QLLaMA, enabling more effective alignment between visual and language modalities. Although the original InternVL-7B already demonstrates strong performance, the integration of MCA further enhances its performance. Additionally, experiments were conducted on the larger LLaVA-1.5-13B model. As shown in the table, MCA can obtain performance enhancement under different scale models, proving its robustness. Results indicate that MCA continues to mitigate hallucinations as model scale increases, further demonstrating its robustness.

Ablation Study of Position Index Settings As shown in Figure 6 and Table 5, MCA-LLaVA preserves two-dimensional local spatial features by assigning the origin of position coordinates to the tokens at the four corners of the image and computing the Manhattan relative distance between tokens. We conduct two sets of ablation studies to verify the effectiveness of this coordinate assignment strategy: (1) setting both the image center and the four corners as origins; (2) setting only the image center as the origin. The results in Table 5 confirm that the coordinate design in MCA is the optimal configuration. In addition, compared with the CCA and Reverse Raster-scan settings, our method improves position modeling and addresses the long-range decay of RoPE through a relative position computation mechanism, rather than relying on heuristic position reassignments, making it more effective and interpretable.

Method	Num	POPE		CHAIR		
		F1 score \uparrow	acc \uparrow	$C_S \downarrow$	$C_I \downarrow$	Recall \uparrow
Raster-scan	526	79.3	79.8	47.0	13.8	76.6
Reverse Raster-scan	526	76.1	76.6	48.1	14.1	75.2
CCA	12	85.9	86.5	43.0	11.5	80.4
Variant of MCA	12	81.3	81.2	52.4	14.2	81.9
Reverse MCA	23	80.8	81.2	50.8	14.4	74.9
MCA	23	86.0 (+6.7)	86.5 (+6.7)	38.0 (+9.0)	10.9 (+2.9)	76.6

Table 5: Ablation experiments under different positional coding methods and MCA variants. Num denotes the number of image tokens positional indexes.

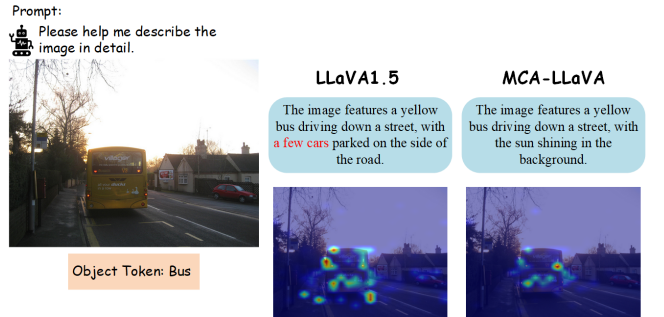


Figure 7: Attention Maps Visualization of MCA.

Attention Maps Visualization of MCA We further analyze heatmaps over the image for object tokens to investigate the model’s differences in visual perception. As shown in the Figure 7, compared to the baseline, MCA-LLaVA demonstrates increased attention to local features of objects and enhanced perception of other regions in the image. We hypothesize that MCA helps improve the model’s visual perception capabilities, including both global context and local details, thereby contributing to the mitigation of hallucinations.

5 Conclusion

This paper provides an in-depth analysis of the limitations of the one-dimensional long-term decay of RoPE: the long-term decay induces image alignment bias, where image tokens distant from the instruction tokens are considered unimportant. With the help of information flow, we find that image alignment bias hinders cross-modal alignment and makes LVLMS more prone to hallucinations. To this end, we improve the RoPE relative position calculation mechanism and propose the Manhattan Causal Attention (MCA). The results of multiple evaluation benchmarks demonstrate the effectiveness of MCA.

References

- [1] Josh Achiam, Steven Adler, Sandhini Agarwal, Lama Ahmad, Ilge Akkaya, Florencia Leoni Aleman, Diogo Almeida, Janko Altenschmidt, Sam Altman, Shyamal Anadkat, et al. 2023. Gpt-4 technical report. *arXiv preprint arXiv:2303.08774* (2023).
- [2] Wenbin An, Feng Tian, Sicong Leng, Jiahao Nie, Haonan Lin, QianYing Wang, Guang Dai, Ping Chen, and Shijian Lu. 2024. AGLA: Mitigating Object Hallucinations in Large Vision-Language Models with Assembly of Global and Local Attention. *arXiv preprint arXiv:2406.12718* (2024).
- [3] Jinze Bai, Shuai Bai, Shusheng Yang, Shijie Wang, Sinan Tan, Peng Wang, Junyang Lin, Chang Zhou, and Jingren Zhou. 2023. Qwen-vl: A frontier large vision-language model with versatile abilities. *arXiv preprint arXiv:2308.12966* (2023).
- [4] Zechen Bai, Pichao Wang, Tianjun Xiao, Tong He, Zongbo Han, Zheng Zhang, and Mike Zheng Shou. 2024. Hallucination of Multimodal Large Language Models: A Survey. *ArXiv abs/2404.18930* (2024).
- [5] Beitao Chen, Xinyu Lyu, Lianli Gao, Jingkuan Song, and Hengtao Shen. 2024. Alleviating Hallucinations in Large Vision-Language Models through Hallucination-Induced Optimization. *ArXiv abs/2405.15356* (2024).
- [6] Cong Chen, Mingyu Liu, Chenchen Jing, Yizhou Zhou, Fengyun Rao, Hao Chen, Bo Zhang, and Chunhua Shen. 2025. PerturboLLaVA: Reducing Multimodal Hallucinations with Perturbative Visual Training.
- [7] Lin Chen, Jinsong Li, Xiao wen Dong, Pan Zhang, Yuhang Zang, Zehui Chen, Haodong Duan, Jiaqi Wang, Yu Qiao, Dahua Lin, and Feng Zhao. 2024. Are We on the Right Way for Evaluating Large Vision-Language Models? *ArXiv abs/2403.20330* (2024).
- [8] Liang Chen, Haozhe Zhao, Tianyu Liu, Shuai Bai, Junyang Lin, Chang Zhou, and Baobao Chang. 2024. An image is worth 1/2 tokens after layer 2: Plug-and-play inference acceleration for large vision-language models. *18th European Conference on Computer Vision ECCV 2024* (2024).
- [9] Zhe Chen, Jiannan Wu, Wenhai Wang, Weijie Su, Guo Chen, Sen Xing, Muyan Zhong, Qinglong Zhang, Xizhou Zhu, Lewei Lu, et al. 2024. Internvl: Scaling up vision foundation models and aligning for generic visual-linguistic tasks. In *Proceedings of the IEEE/CVF Conference on Computer Vision and Pattern Recognition*. 24185–24198.
- [10] Zhaorun Chen, Zhuokai Zhao, Hongyin Luo, Huaxiu Yao, Bo Li, and Jiawei Zhou. 2024. HALC: Object Hallucination Reduction via Adaptive Focal-Contrast Decoding. *arXiv preprint arXiv:2403.00425* (2024).
- [11] Wei-Lin Chiang, Zhuohan Li, Zi Lin, Ying Sheng, Zhanghao Wu, Hao Zhang, Lianmin Zheng, Siyuan Zhuang, Yonghao Zhuang, Joseph E Gonzalez, et al. 2023. Vicuna: An open-source chatbot impressing gpt-4 with 90%* chatgpt quality. See <https://vicuna.lmsys.org> (accessed 14 April 2023) 2, 3 (2023), 6.
- [12] Yung-Sung Chuang, Yujia Xie, Hongyin Luo, Yoon Kim, James Glass, and Pengcheng He. 2023. Dola: Decoding by contrasting layers improves factuality in large language models. *arXiv preprint arXiv:2309.03883* (2023).
- [13] Chenhang Cui, An Zhang, Yiyang Zhou, Zhaorun Chen, Gelei Deng, Huaxiu Yao, and Tat-Seng Chua. 2024. Fine-Grained Verifiers: Preference Modeling as Next-token Prediction in Vision-Language Alignment. *ArXiv abs/2410.14148* (2024).
- [14] Jacob Devlin, Ming-Wei Chang, Kenton Lee, and Kristina Toutanova. 2018. Bert: Pre-training of deep bidirectional transformers for language understanding. *arXiv preprint arXiv:1810.04805* (2018).
- [15] Alexey Dosovitskiy, Lucas Beyer, Alexander Kolesnikov, Dirk Weissenborn, Xi-aohua Zhai, Thomas Unterthiner, Mostafa Dehghani, Matthias Minderer, Georg Heigold, Sylvain Gelly, Jakob Uszkoreit, and Neil Houlsby. 2021. An Image is Worth 16x16 Words: Transformers for Image Recognition at Scale. *ICLR* (2021).
- [16] Yuhang Fu, Ruobing Xie, Xingwu Sun, Zhanhui Kang, and Xirong Li. 2024. Mitigating Hallucination in Multimodal Large Language Model via Hallucination-targeted Direct Preference Optimization. *ArXiv abs/2411.10436* (2024).
- [17] Xuan Gong, Tianshi Ming, Xinpeng Wang, and Zhihua Wei. 2024. DAMRO: Dive into the Attention Mechanism of LVLm to Reduce Object Hallucination. In *Conference on Empirical Methods in Natural Language Processing*.
- [18] Yash Goyal, Tejas Khot, Douglas Summers-Stay, Dhruv Batra, and Devi Parikh. 2016. Making the V in VQA Matter: Elevating the Role of Image Understanding in Visual Question Answering. *International Journal of Computer Vision* 127 (2016), 398 – 414.
- [19] Anisha Gunjal, Jihan Yin, and Erhan Bas. 2024. Detecting and preventing hallucinations in large vision language models. In *Proceedings of the AAAI Conference on Artificial Intelligence*, Vol. 38. 18135–18143.
- [20] Danna Gurari, Qing Li, Abigale J Stangl, Anhong Guo, Chi Lin, Kristen Grauman, Jiebo Luo, and Jeffrey P Bigham. 2018. Vizwiz grand challenge: Answering visual questions from blind people. In *Proceedings of the IEEE conference on computer vision and pattern recognition*. 3608–3617.
- [21] Xin He, Longhui Wei, Lingxi Xie, and Qi Tian. 2024. Incorporating Visual Experts to Resolve the Information Loss in Multimodal Large Language Models. *ArXiv abs/2401.03105* (2024).
- [22] Qidong Huang, Xiaoyi Dong, Pan Zhang, Bin Wang, Conghui He, Jiaqi Wang, Dahua Lin, Weiming Zhang, and Nenghai Yu. 2024. Opera: Alleviating hallucination in multi-modal large language models via over-trust penalty and retrospection-allocation. In *Proceedings of the IEEE/CVF Conference on Computer Vision and Pattern Recognition*. 13418–13427.
- [23] Zhiheng Huang, Davis Liang, Peng Xu, and Bing Xiang. 2020. Improve Transformer Models with Better Relative Position Embeddings. In *Findings of the Association for Computational Linguistics: EMNLP 2020*. 3327–3335.
- [24] Drew A Hudson and Christopher D Manning. 2019. Gqa: A new dataset for real-world visual reasoning and compositional question answering. In *Proceedings of the IEEE/CVF conference on computer vision and pattern recognition*. 6700–6709.
- [25] Fushuo Huo, Wenchao Xu, Zhong Zhang, Haozhao Wang, Zhicheng Chen, and Peilin Zhao. 2025. Self-Introspective Decoding: Alleviating Hallucinations for Large Vision-Language Models. In *The Thirteenth International Conference on Learning Representations*.
- [26] Chaoya Jiang, Haiyang Xu, Mengfan Dong, Jiaxing Chen, Wei Ye, Mingshi Yan, Qinghao Ye, Ji Zhang, Fei Huang, and Shikun Zhang. 2023. Hallucination Augmented Contrastive Learning for Multimodal Large Language Model. *2024 IEEE/CVF Conference on Computer Vision and Pattern Recognition (CVPR)* (2023), 27026–27036.
- [27] Junho Kim, Hyunjun Kim, Yeonju Kim, and Yonghyun Ro. 2024. CODE: Contrasting Self-generated Description to Combat Hallucination in Large Multi-modal Models. *ArXiv abs/2406.01920* (2024).
- [28] Sihyeon Kim, Boryeong Cho, Sangmin Bae, Sumyeong Ahn, and SeYoung Yun. 2024. VACoDe: Visual Augmented Contrastive Decoding. *ArXiv abs/2408.05337* (2024).
- [29] Sicong Leng, Yun Xing, Zesen Cheng, Yang Zhou, Hang Zhang, Xin Li, Deli Zhao, Shijian Lu, Chunyan Miao, and Li Bing. 2024. The Curse of Multi-Modalities: Evaluating Hallucinations of Large Multimodal Models across Language, Visual, and Audio. *ArXiv abs/2410.12787* (2024).
- [30] Sicong Leng, Hang Zhang, Guanzheng Chen, Xin Li, Shijian Lu, Chunyan Miao, and Lidong Bing. 2024. Mitigating object hallucinations in large vision-language models through visual contrastive decoding. In *Proceedings of the IEEE/CVF Conference on Computer Vision and Pattern Recognition*. 13872–13882.
- [31] Bohao Li, Rui Wang, Guangzhi Wang, Yuying Ge, Yixiao Ge, and Ying Shan. 2023. SEED-Bench: Benchmarking Multimodal LLMs with Generative Comprehension. *ArXiv abs/2307.16125* (2023).
- [32] Chunyuan Li, Cliff Wong, Sheng Zhang, Naoto Usuyama, Haotian Liu, Jianwei Yang, Tristan Naumann, Hoifung Poon, and Jianfeng Gao. 2024. Llava-med: Training a large language-and-vision assistant for biomedicine in one day. *Advances in Neural Information Processing Systems* 36 (2024).
- [33] Kenneth Li, Oam Patel, Fernanda Viégas, Hanspeter Pfister, and Martin Wattenberg. 2024. Inference-time intervention: Eliciting truthful answers from a language model. *Advances in Neural Information Processing Systems* 36 (2024).
- [34] Yifan Li, Yifan Du, Kun Zhou, Jinpeng Wang, Wayne Xin Zhao, and Ji-Rong Wen. 2023. Evaluating object hallucination in large vision-language models. *arXiv preprint arXiv:2305.10355* (2023).
- [35] Yifan Li, Yifan Du, Kun Zhou, Jinpeng Wang, Wayne Xin Zhao, and Ji-Rong Wen. 2023. Evaluating object hallucination in large vision-language models. *arXiv preprint arXiv:2305.10355* (2023).
- [36] Zhuowei Li, Haizhou Shi, Yunhe Gao, Di Liu, Zhenting Wang, Yuxiao Chen, Ting Liu, Long Zhao, Hao Wang, and Dimitris N. Metaxas. 2025. The Hidden Life of Tokens: Reducing Hallucination of Large Vision-Language Models via Visual Information Steering. *ArXiv abs/2502.03628* (2025).
- [37] Fuxiao Liu, Kevin Lin, Linjie Li, Jianfeng Wang, Yaser Yacoob, and Lijuan Wang. 2023. Mitigating Hallucination in Large Multi-Modal Models via Robust Instruction Tuning. In *International Conference on Learning Representations*.
- [38] Haotian Liu, Chunyuan Li, Yuheng Li, and Yong Jae Lee. 2023. Improved Baselines with Visual Instruction Tuning. *2024 IEEE/CVF Conference on Computer Vision and Pattern Recognition (CVPR)* (2023), 26286–26296.
- [39] Haotian Liu, Chunyuan Li, Qingyang Wu, and Yong Jae Lee. 2024. Visual Instruction Tuning. *Advances in neural information processing systems* 36 (2024).
- [40] Hanchao Liu, Wenyuan Xue, Yifei Chen, Dapeng Chen, Xiutian Zhao, Ke Wang, Liping Hou, Rong-Zhi Li, and Wei Peng. 2024. A Survey on Hallucination in Large Vision-Language Models. *ArXiv abs/2402.00253* (2024).
- [41] Shiping Liu, Kecheng Zheng, and Wei Chen. 2024. Paying More Attention to Image: A Training-Free Method for Alleviating Hallucination in LVLms. *ArXiv abs/2407.21771* (2024).
- [42] Pan Lu, Swaroop Mishra, Tanglin Xia, Liang Qiu, Kai-Wei Chang, Song-Chun Zhu, Oyvind Tafjord, Peter Clark, and Ashwin Kalyan. 2022. Learn to explain: Multimodal reasoning via thought chains for science question answering. *Advances in Neural Information Processing Systems* 35 (2022), 2507–2521.
- [43] Minesh Mathew, Dimosthenis Karatzas, R. Manmatha, and C. V. Jawahar. 2020. DocVQA: A Dataset for VQA on Document Images. *2021 IEEE Winter Conference on Applications of Computer Vision (WACV)* (2020), 2199–2208.
- [44] Renjie Pi, Tianyang Han, Wei Xiong, Jipeng Zhang, Runtao Liu, Rui Pan, and Tong Zhang. 2024. Strengthening Multimodal Large Language Model with Bootstrapped Preference Optimization. *ArXiv abs/2403.08730* (2024).

- [45] Alec Radford, Jong Wook Kim, Chris Hallacy, Aditya Ramesh, Gabriel Goh, Sandhini Agarwal, Girish Sastry, Amanda Askell, Pamela Mishkin, Jack Clark, et al. 2021. Learning transferable visual models from natural language supervision. In *International conference on machine learning*. PMLR, 8748–8763.
- [46] Anna Rohrbach, Lisa Anne Hendricks, Kaylee Burns, Trevor Darrell, and Kate Saenko. 2018. Object hallucination in image captioning. *arXiv preprint arXiv:1809.02156* (2018).
- [47] Pritam Sarkar, Sayna Ebrahimi, Ali Etemad, Ahmad Beirami, Sercan Ö. Arik, and Tomas Pfister. 2024. Mitigating Object Hallucination in MLLMs via Data-augmented Phrase-level Alignment.
- [48] Yuying Shang, Xinyi Zeng, Yutao Zhu, Xiao Yang, Zhengwei Fang, Jingyuan Zhang, Jiawei Chen, Zinan Liu, and Yu Tian. 2024. From Pixels to Tokens: Revisiting Object Hallucinations in Large Vision-Language Models. *ArXiv abs/2410.06795* (2024).
- [49] Amanpreet Singh, Vivek Natarajan, Meet Shah, Yu Jiang, Xinlei Chen, Dhruv Batra, Devi Parikh, and Marcus Rohrbach. 2019. Towards VQA Models That Can Read. *2019 IEEE/CVF Conference on Computer Vision and Pattern Recognition (CVPR)* (2019), 8309–8318.
- [50] Jianlin Su, Yu Lu, Shengfeng Pan, Bo Wen, and Yunfeng Liu. 2021. RoFormer: Enhanced Transformer with Rotary Position Embedding. *ArXiv abs/2104.09864* (2021).
- [51] Zhiqing Sun, Sheng Shen, Shengcao Cao, Haotian Liu, Chunyuan Li, Yikang Shen, Chuang Gan, Liang-Yan Gui, Yu-Xiong Wang, Yiming Yang, et al. 2023. Aligning large multimodal models with factually augmented rlhf. *arXiv preprint arXiv:2309.14525* (2023).
- [52] Feilong Tang, Zile Huang, Chengzhi Liu, Qiang Sun, Harry Yang, and Ser-Nam Lim. 2025. Intervening anchor token: Decoding strategy in alleviating hallucinations for MLLMs. In *The Thirteenth International Conference on Learning Representations*.
- [53] Feilong Tang, Zile Huang, Chengzhi Liu, Qiang Sun, Harry Yang, and Ser-Nam Lim. 2025. Intervening Anchor Token: Decoding Strategy in Alleviating Hallucinations for MLLMs. In *The Thirteenth International Conference on Learning Representations*.
- [54] Feilong Tang, Chengzhi Liu, Zhongxing Xu, Ming Hu, Zile Huang, Haochen Xue, Ziyang Chen, Zelin Peng, Zhiwei Yang, Sijin Zhou, et al. 2025. Seeing Far and Clearly: Mitigating Hallucinations in MLLMs with Attention Causal Decoding. In *Proceedings of the Computer Vision and Pattern Recognition Conference*. 26147–26159.
- [55] Hugo Touvron, Thibaut Lavril, Gautier Izacard, Xavier Martinet, Marie-Anne Lachaux, Timothée Lacroix, Baptiste Rozière, Naman Goyal, Eric Hambro, Faisal Azhar, Aurélien Rodriguez, Armand Joulin, Edouard Grave, and Guillaume Lample. 2023. LLaMA: Open and Efficient Foundation Language Models. *ArXiv abs/2302.13971* (2023).
- [56] Ashish Vaswani, Noam M. Shazeer, Niki Parmar, Jakob Uszkoreit, Llion Jones, Aidan N. Gomez, Lukasz Kaiser, and Illia Polosukhin. 2017. Attention is All you Need. In *Neural Information Processing Systems*.
- [57] Fei Wang, Wenxuan Zhou, James Y. Huang, Nan Xu, Sheng Zhang, Hoifung Poon, and Muhao Chen. 2024. mDPO: Conditional Preference Optimization for Multimodal Large Language Models. *ArXiv abs/2406.11839* (2024).
- [58] Jiaqi Wang, Yifei Gao, and Jitao Sang. 2024. VaLiD: Mitigating the Hallucination of Large Vision Language Models by Visual Layer Fusion Contrastive Decoding. *ArXiv abs/2411.15839* (2024).
- [59] Lei Wang, Jiabang He, Shenshen Li, Ning Liu, and Ee-Peng Lim. 2023. Mitigating Fine-Grained Hallucination by Fine-Tuning Large Vision-Language Models with Caption Rewrites. In *Conference on Multimedia Modeling*.
- [60] Lean Wang, Lei Li, Damai Dai, Deli Chen, Hao Zhou, Fandong Meng, Jie Zhou, and Xu Sun. 2023. Label words are anchors: An information flow perspective for understanding in-context learning. *arXiv preprint arXiv:2305.14160* (2023).
- [61] Peng Wang, Shuai Bai, Sinan Tan, Shijie Wang, Zhihao Fan, Jinze Bai, Keqin Chen, Xuejing Liu, Jialin Wang, Wenbin Ge, Yang Fan, Kai Dang, Mengfei Du, Xuancheng Ren, Rui Men, Dayiheng Liu, Chang Zhou, Jingren Zhou, and Junyang Lin. 2024. Qwen2-VL: Enhancing Vision-Language Model’s Perception of the World at Any Resolution. *arXiv preprint arXiv:2409.12191* (2024).
- [62] Xintong Wang, Jingheng Pan, Liang Ding, and Christian Biemann. 2024. Mitigating Hallucinations in Large Vision-Language Models with Instruction Contrastive Decoding. *ArXiv abs/2403.18715* (2024).
- [63] Zhaoyang Wang, Weilei He, Zhiyuan Liang, Xuchao Zhang, Chetan Bansal, Ying Wei, Weitong Zhang, and Huaxiu Yao. 2024. CREAM: Consistency Regularized Self-Rewarding Language Models. *ArXiv abs/2410.12735* (2024).
- [64] Jinfeng Wei and Xiaofeng Zhang. 2024. DOPRA: Decoding Over-accumulation Penalization and Re-allocation in Specific Weighting Layer. *Proceedings of the 32nd ACM International Conference on Multimedia* (2024).
- [65] Yuxi Xie, Guanzhen Li, Xiao Xu, and Min-Yen Kan. 2024. V-DPO: Mitigating Hallucination in Large Vision Language Models via Vision-Guided Direct Preference Optimization. In *Conference on Empirical Methods in Natural Language Processing*.
- [66] Yun Xing, Yiheng Li, Ivan Laptev, and Shijian Lu. 2024. Mitigating Object Hallucination via Concentric Causal Attention. *arXiv preprint arXiv:2410.15926* (2024).
- [67] Tianyi Xiong, Xiyao Wang, Dong Guo, Qinghao Ye, Haoqi Fan, Quanquan Gu, Heng Huang, and Chunyuan Li. 2024. LLaVA-Critic: Learning to Evaluate Multimodal Models. *ArXiv abs/2410.02712* (2024).
- [68] Haochen Xue, Feilong Tang, Ming Hu, Yexin Liu, Qidong Huang, Yulong Li, Chengzhi Liu, Zhongxing Xu, Chong Zhang, Chun-Mei Feng, et al. 2025. Mmrc: A large-scale benchmark for understanding multimodal large language model in real-world conversation. *arXiv preprint arXiv:2502.11903* (2025).
- [69] Qinghao Ye, Haiyang Xu, Jiabo Ye, Ming Yan, Anwen Hu, Haowei Liu, Qi Qian, Ji Zhang, and Fei Huang. 2024. mplug-owl2: Revolutionizing multi-modal large language model with modality collaboration. In *Proceedings of the IEEE/CVF Conference on Computer Vision and Pattern Recognition*. 13040–13051.
- [70] Hao Yin, Guangzong Si, and Zilei Wang. 2025. ClearSight: Visual Signal Enhancement for Object Hallucination Mitigation in Multimodal Large language Models. (2025).
- [71] Shukang Yin, Chaoyou Fu, Sirui Zhao, Ke Li, Xing Sun, Tong Xu, and Enhong Chen. 2023. A survey on multimodal large language models. *arXiv preprint arXiv:2306.13549* (2023).
- [72] Qifan Yu, Juncheng Li, Longhui Wei, Liang Pang, Wentao Ye, Bosheng Qin, Siliang Tang, Qi Tian, and Yueting Zhuang. 2023. HalluciDoctor: Mitigating Hallucinatory Toxicity in Visual Instruction Data. *2024 IEEE/CVF Conference on Computer Vision and Pattern Recognition (CVPR)* (2023), 12944–12953.
- [73] Tianyu Yu, Yuan Yao, Haoye Zhang, Taiwan He, Yifeng Han, Ganqu Cui, Jinyi Hu, Zhiyuan Liu, Hai-Tao Zheng, Maosong Sun, et al. 2023. RLhf-v: Towards trustworthy mlms via behavior alignment from fine-grained correctional human feedback. *arXiv preprint arXiv:2312.00849* (2023).
- [74] Weihao Yu, Zhengyuan Yang, Linjie Li, Jianfeng Wang, Kevin Lin, Zicheng Liu, Xinchao Wang, and Lijuan Wang. 2023. Mm-vet: Evaluating large multimodal models for integrated capabilities. *arXiv preprint arXiv:2308.02490* (2023).
- [75] Zhongzhi Yu, Zheng Wang, Yonggan Fu, Huihong Shi, Khalid Shaikh, and Yingyan Celine Lin. 2024. Unveiling and Harnessing Hidden Attention Sinks: Enhancing Large Language Models without Training through Attention Calibration. *arXiv preprint arXiv:2406.15765* (2024).
- [76] Zihao Yue, Liang Zhang, and Qin Jin. 2024. Less is more: Mitigating multimodal hallucination from an eos decision perspective. *The 62nd Annual Meeting of the Association for Computational Linguistics* (2024).
- [77] Hang Zhang, Xin Li, and Lidong Bing. 2023. Video-llama: An instruction-tuned audio-visual language model for video understanding. *arXiv preprint arXiv:2306.02858* (2023).
- [78] Jinrui Zhang, Teng Wang, Haigang Zhang, Ping Lu, and Feng Zheng. 2024. Reflective Instruction Tuning: Mitigating Hallucinations in Large Vision-Language Models. *ArXiv abs/2407.11422* (2024).
- [79] Shilong Zhang, Peize Sun, Shoufa Chen, Min Xiao, Wenqi Shao, Wenwei Zhang, Kai Chen, and Ping Luo. 2023. Gpt4roi: Instruction tuning large language model on region-of-interest. *arXiv preprint arXiv:2307.03601* (2023).
- [80] Xiaofeng Zhang, Yihao Quan, Haochen Gu, Chen Shen, Xiaosong Yuan, Shaotian Yan, Hao Cheng, Kaijie Wu, and Jieping Ye. 2024. Seeing Clearly by Layer Two: Enhancing Attention Heads to Alleviate Hallucination in LVLs. *ArXiv abs/2411.09968* (2024).
- [81] Xiaofeng Zhang, Chen Shen, Xiaosong Yuan, Shaotian Yan, Liang Xie, Wenxiao Wang, Haochen Gu, Hao Tang, and Jieping Ye. 2024. From Redundancy to Relevance: Enhancing Explainability in Multimodal Large Language Models. *arXiv preprint arXiv:2406.06579* (2024).
- [82] Xiaofeng Zhang, Fanshuo Zeng, and Haochen Gu. 2024. Simignore: Exploring and enhancing multimodal large model complex reasoning via similarity computation. *Neural Networks* (2024), 107059.
- [83] Xiaofeng Zhang, Fanshuo Zeng, Yihao Quan, Zheng Hui, and Jiawei Yao. 2025. Enhancing Multimodal Large Language Models Complex Reason via Similarity Computation. *AAAI* (2025).
- [84] Yiyang Zhou, Chenhang Cui, Jaehong Yoon, Linjun Zhang, Zhun Deng, Chelsea Finn, Mohit Bansal, and Huaxiu Yao. 2023. Analyzing and mitigating object hallucination in large vision-language models. *arXiv preprint arXiv:2310.00754* (2023).
- [85] Yiyang Zhou, Zhiyuan Fan, Dongjie Cheng, Sihan Yang, Zhaorun Chen, Chenhang Cui, Xiyao Wang, Yun Li, Linjun Zhang, and Huaxiu Yao. 2024. Calibrated Self-Rewarding Vision Language Models. *ArXiv abs/2405.14622* (2024).
- [86] Deyao Zhu, Jun Chen, Xiaoqian Shen, Xiang Li, and Mohamed Elhoseiny. 2023. Minigpt-4: Enhancing vision-language understanding with advanced large language models. *arXiv preprint arXiv:2304.10592* (2023).
- [87] Lanyun Zhu, Deyi Ji, Tianrun Chen, Peng Xu, Jieping Ye, and Jun Liu. 2024. IBD: Alleviating Hallucinations in Large Vision-Language Models via Image-Biased Decoding. *ArXiv abs/2402.18476* (2024).
- [88] Tinghui Zhu, Qin Liu, Fei Wang, Zhengzhong Tu, and Muhao Chen. 2024. Unraveling Cross-Modality Knowledge Conflicts in Large Vision-Language Models. *ArXiv abs/2410.03659* (2024).
- [89] Younan Zhu, Linwei Tao, Mingjing Dong, and Chang Xu. 2025. Mitigating Object Hallucinations in Large Vision-Language Models via Attention Calibration. *ArXiv abs/2502.01969* (2025).